Apolipoprotein L1 confers pH-switchable ion permeability to phospholipid vesicles

Received for publication, August 18, 2017, and in revised form, September 8, 2017 Published, Papers in Press, September 15, 2017, DOI 10.1074/jbc.M117.813444

Jonathan Bruno[‡], Nicola Pozzi[§], Jonathan Oliva[§], and John C. Edwards[‡1]

From the Departments of [‡]Internal Medicine and [§]Biochemistry and Molecular Biology, Saint Louis University, St. Louis, Missouri 63110

Edited by George M. Carman

Apolipoprotein L1 (ApoL1) is a human serum protein conferring resistance to African trypanosomes, and certain ApoL1 variants increase susceptibility to some progressive kidney diseases. ApoL1 has been hypothesized to function like a pore-forming colicin and has been reported to have permeability effects on both intracellular and plasma membranes. Here, to gain insight into how ApoL1 may function *in vivo*, we used vesicle-based ion permeability, direct membrane association, and intrinsic fluorescence to study the activities of purified recombinant ApoL1. We found that ApoL1 confers chloride-selective permeability to preformed phospholipid vesicles and that this selectivity is strongly pH-sensitive, with maximal activity at pH 5 and little activity above pH 7. When ApoL1 and lipid were allowed to interact at low pH and were then brought to neutral pH, chloride permeability was suppressed, and potassium permeability was activated. Both chloride and potassium permeability linearly correlated with the mass of ApoL1 in the reaction mixture, and both exhibited lipid selectivity, requiring the presence of negatively charged lipids for activity. Potassium, but not chloride, permease activity required the presence of calcium ions in both the association and activation steps. Direct assessment of ApoL1–lipid associations confirmed that ApoL1 stably associates with phospholipid vesicles, requiring low pH and the presence of negatively charged phospholipids for maximal binding. Intrinsic fluorescence of ApoL1 supported the presence of a significant structural transition when ApoL1 is mixed with lipids at low pH. This pH-switchable ion-selective permeability may explain the different effects of ApoL1 reported in intracellular and plasma membrane environments.

Variants in apolipoprotein L1 (ApoL1)[2] have been shown to be responsible for the increased risk of certain progressive kidney diseases in populations of African ancestry (1, 2). However, the role of normal ApoL1 in the kidney and the mechanisms by which the variants exacerbate disease are uncertain. Clarification of the biochemical properties and activities of the ApoL1 protein should illuminate possible mechanisms of kidney injury and may lead to potential therapies.

Prior to recognition of its role in kidney disease, ApoL1 was known to be a serum protein that confers resistance to infection by *Trypanosoma brucei* (3, 4). Based on homology to bacterial colicins, it has been hypothesized that ApoL1 kills trypanosomes by being endocytosed into the trypanosomal vacuole, where the low pH level induces a conformational change in the molecule, allowing direct insertion in the vacuolar membrane, where it can function as an ion channel (5, 6). Initial reports supported the hypothesis that ApoL1 functions as an anion channel in the vacuolar membrane, leading to dysfunction or disruption of the vacuolar compartment and eventual parasite death (5), and subsequent data support the hypothesis that ApoL1 has direct effects on the endocytic pathway (7). However, published data demonstrating anion-selective channel activity of ApoL1 are rather sparse.

There are only two reports in the literature directly demonstrating anion channel activity associated with ApoL1 (5, 8). The first study used an internal segment of the ApoL1 sequence that had been modeled to function as a pore-forming region based on similarity to colicin A. This peptide was shown to generate non-rectifying, modestly chloride-selective channels in planar lipid bilayers. Single-channel conductance transitions were between 2.5 and 10 picosiemens in 300 mM KCl, and the chloride-to-potassium permeability ratio was 3.2:1. Furthermore, these investigators reconstituted full-length ApoL1 into lipid membranes by detergent dialysis at neutral pH. They demonstrated ^{36}Cl uptake that was not inhibited by the chloride channel inhibitor DIDS and was greater when assayed at pH 5 than at pH 7. A second report by another group used full-length ApoL1 purified from human serum (8). These investigators demonstrated an activity that generated pores in phospholipid vesicles that allowed passage of calcein, a 623-molecular weight molecule that carries four negative charges at neutral pH. This activity required low pH, the presence of negatively charged phospholipid in the vesicle membranes, and low ionic strength to allow ApoL1 to physically associate with vesicles and form pores.

More recently, another group has reported dramatically different results using recombinant ApoL1 refolded from bacterial

This work was supported in part by National Institutes of Health Grant RO1 HL092131 (to J. C. E.). The authors declare that they have no conflicts of interest with the contents of this article. The content is solely the responsibility of the authors and does not necessarily represent the official views of the National Institutes of Health.

[1] To whom correspondence should be addressed: Renal Division/Dept. of Internal Medicine, Saint Louis University, 3635 Vista Ave., St. Louis, MO 63110. Tel.: 314-577-8765; E-mail: edwardjc@slu.edu.

[2] The abbreviations used are: ApoL1, apolipoprotein L1; DIDS, 4,4′-diisothiocyanostilbene-2,2′-disulfonic acid; DDM, dodecyl maltoside; val, valinomycin; Cl1, chloride ionophore 1; PC, 90% phosphatidyl choline, 10% cholesterol; PA, 80% phosphatidyl choline, 10% phosphatidic acid, 10% cholesterol; PS, 80% phosphatidyl choline, 10% phosphatidyl serine, 10% cholesterol; PE, 80% phosphatidyl choline, 10% phosphatidyl ethanolamine, 10% cholesterol; ANOVA, analysis of variance; LC_{50}, lethal concentration at which 50% of the population is killed.

inclusion bodies (6). Their channel activity assays exclusively used a lipid bilayer approach. After denaturation and refolding, followed by purification, these investigators reported that ApoL1 requires low pH to insert into membranes but then functions as a non-selective cation channel only after the pH is brought to 7 or higher. In their model, ApoL1 inserts into the vacuolar membrane at low pH and is trafficked to the plasma membrane, where exposure to the neutral extracellular pH activates the cation channel activity, depolarizing and killing the trypanosome. A recent publication (9) demonstrating that mammalian cells expressing ApoL1 show increased plasma membrane non-selective cation permeability that contributes to cell toxicity supports this model. In sum, the transport properties of ApoL1 are unclear from the literature, with one report describing anion-selective permeability at low pH, one reporting permease activity allowing passage of rather large negatively charged molecules at low pH, and one reporting cation channel activity that requires low pH for membrane insertion but only functions at neutral pH.

We have directly investigated the ability of purified recombinant ApoL1 to support the ion permeability of phospholipid membranes. We find that soluble recombinant ApoL1 confers chloride-selective permeability when allowed to insert into vesicles and assayed at low pH but confers potassium permeability when inserted at low pH but assayed at neutral pH. Both activities are linearly related to the mass of ApoL1 in the assays, and both require the presence of negatively charged phospholipids in the membrane vesicles. The potassium permease activity, but not the chloride permease activity, requires the presence of calcium. We assessed the association of ApoL1 with vesicles and found that ApoL1 associates stably with preformed membrane vesicles. Association is dependent on pH and phospholipid composition, similar to the activity assays. Finally, the intrinsic fluorescence of ApoL1 supports the presence of a significant structural change in ApoL1 in the pH range at which membrane insertion is activated. These data suggest a model in which ApoL1, through supporting pH-switchable ion-selective permeability, may mediate the different effects reported in both intracellular and plasma membrane environments.

Results

Purification of denatured and refolded N-terminal His-tagged ApoL1

We adopted the expression, denaturation/refolding, and purification strategy of Thomson and Finkelstein (6), with minor modifications as described under "Experimental procedures." Coomassie-stained gels and the total protein concentration of fractions across the S200 eluate are shown in Fig. 1, *A* and *B*. The product elutes with an apparent molecular mass of about 95 kDa in the presence of 0.02% dodecyl maltoside (DDM), and the peak fractions appear to be essentially pure by protein-stained gel. DDM micelles are reported to be about 70 kDa, suggesting that the protein is either eluting as a micelle-associated monomer or as a dimer that is not embedded in micelles. The protein concentration of the peak fraction from this preparation is typically in the 100- to 150-μg/ml range.

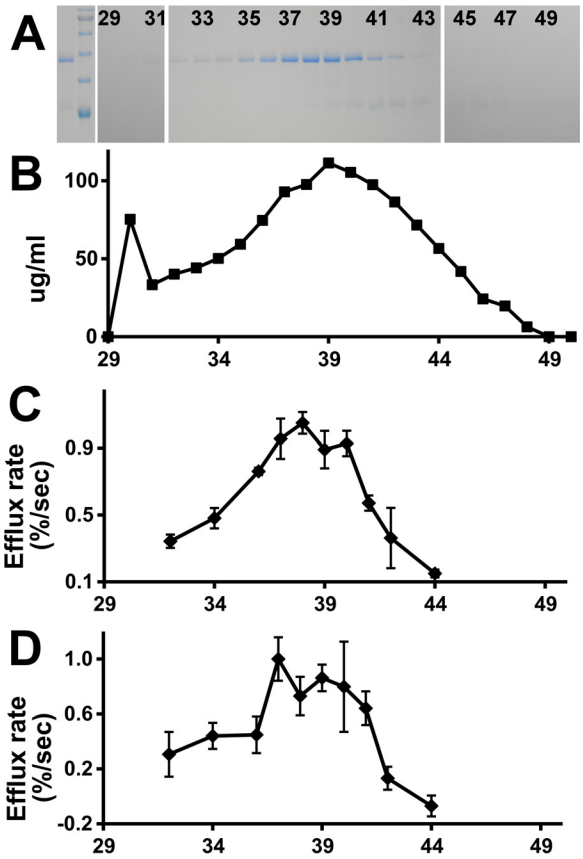

Figure 1. Purification of recombinant His-tagged ApoL1. *A*, protein-stained gel of fractions from purification. *Lane 1*, peak fraction from nickel column elution. *Lane 2*, molecular mass standards (from the top: 100, 75, 63, 48, 35, and 28 kDa). *Lanes 3–23*, fractions 29 through 50 from the S200 column (every other lane is labeled with fraction number). ApoL1 peaks in fractions 38–39, running just below the 48-kDa marker. *B*, protein concentration of S200 fractions. *C*, chloride permease activity of S200 fractions 32–44. Each data point represents the mean, with *error bars* indicating S.E.; $n = 2$ for each. *D*, potassium permease activity of S200 fractions 32–44. Data are as in *C*; $n = 3$ for each data point.

The material was tested for biological activity in a *Trypanosoma brucei brucei* killing curve. *T. brucei* were grown in the presence of a series of dilutions of ApoL1, and trypanosome viability was assessed (Fig. 2). The LC_{50} is 40 ng/ml, which is similar to a value reported previously (6), indicating that this preparation retains its biological activity against trypanosomes.

Ion permease activity of refolded N-terminally tagged ApoL1

We used a vesicle-based efflux approach to characterize the activity of refolded ApoL1 (10). The assay consists of two separate stages. In the association stage, ApoL1 is mixed with KCl-loaded vesicles and allowed to insert into the membranes. Extravesicular KCl is then removed by passage through a desalting spin column equilibrated in isotonic sucrose, generating large inside-to-outside gradients of both potassium and chloride ions. In the efflux stage, the spin column eluate is diluted into an isotonic solution that maintains the KCl gradient. Extravesicular chloride concentration is monitored with a chloride-selective electrode. Even when either a potassium or chloride selective permeability is present, neither ion will be able to exit the vesicles because of lack of counterion movement. Voltage-driven ion efflux is initiated by addition of a

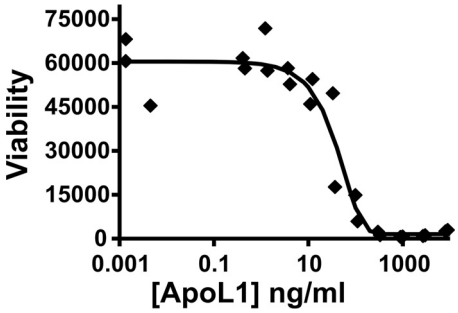

Figure 2. Toxicity of purified recombinant ApoL1 to trypanosomes. The viability of *T. brucei brucei* grown in the presence of ApoL1 is plotted against the ApoL1 concentration on a log scale. The LC_{50} is 40 ng/ml.

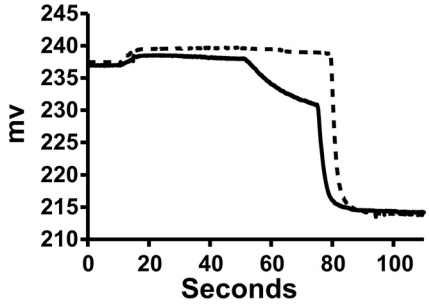

Figure 3. Representative raw data from a chloride permease assays. Traces from the ApoL1 fraction (*solid line*) and control buffer (*dotted line*) are shown. Both the initial reaction mixture and the efflux step were at pH 5.0. The initial recording is of 10^{-5} M KCl, 2 mM $Ca(gluconate)_2$, and 10 mM MES (pH 5.0) in 300 mM sucrose in the cup. The upward deflection at about 10 s reflects addition of the Bio-gel P-6DG eluate with the chloride-loaded vesicles that dilutes the chloride in the cup. Val is added at 60 s, initiating voltage-driven KCl efflux. Triton X-100 is added at 90 s, releasing all remaining intravesicular chloride. The minimal chloride release before addition of val in both tracings indicates that the vesicle potassium permeability is low with or without ApoL1. The difference in initial rates of release after addition of val is taken as the ApoL1-dependent chloride permeability.

counterion ionophore. Addition of the potassium-selective ionophore valinomycin (val) will induce a large inside negative membrane potential that, when chloride permeability is present, will drive KCl efflux which will be detected by the chloride-selective electrode. Conversely, addition of a chloride-selective ionophore will induce an inside positive membrane potential that will drive KCl efflux when potassium permeability is present. Thus, this assay can serve as either a chloride or potassium permeability assay, depending on which ionophore is used. Note that efflux prior to addition of the ionophore reflects permeability to both potassium and chloride.

Chloride permeability assay

Starting from the initial hypothesis that low pH induces a structural transition that allows membrane insertion and chloride channel activity, we mixed purified ApoL1 with vesicles at pH 5 and then assayed for val-driven efflux at pH 5. Representative tracings with either ApoL1 or control buffer are shown in Fig. 3. The difference in rates with and without ApoL1 after addition of val represents the ApoL1-dependent chloride permeability of the vesicles. There are two additional points to note. First, the val-dependent rate in the control vesicles is not zero, indicating that the vesicles themselves have some finite chloride permeability. Second, the very low rate of chloride release prior to addition of val indicates that the potassium permeability is very much lower than the chloride permeability.

Assays were carried out with a range of ApoL1 in the assay, demonstrating a linear relationship between the mass of ApoL1 and activity (Fig. 4*A*). The S200 eluate fractions were assayed for chloride permeability, and the results are shown in Fig. 1*C*. The chloride permease activity co-elutes with the peak of ApoL1 protein. The presence of calcium enhances activity (Fig. 4*B*), although there is substantial activity even in the absence of calcium. Altering the intravesicular (trans) pH between pH 5 and 8 while maintaining the extravesicular (cis) pH at 5 had no effect on activity (data not shown).

Activity as a function of pH is shown in Fig. 4*C*. Both membrane association and efflux were carried out at the indicated pH in the presence of calcium. Chloride permeability is greatest when assayed at pH 5 to 5.5, above which activity rapidly drops, and it is very low above pH 7.0. The effect of pH switch after membrane association is shown in Fig. 4*D*. Membranes and protein were mixed at pH 6 and then assayed for val-driven efflux at various pH values as shown. pH switch to neutral after association suppressed Cl permeability, but there is still detectable chloride permeability after pH switch, even up to pH 8.0.

The composition of the lipid vesicles has a marked effect on ApoL1-associated chloride permeability. Assays were carried out with asolectin vesicles (a complex mixture of soybean phospholipids) or combinations of purified phospholipids. Each of the purified phospholipid mixtures also contained 10% cholesterol to minimize ionic leakiness. The results are shown in Fig. 4*E*. Asolectin vesicles support robust activity. In contrast, ApoL1 confers no significant chloride permeability to vesicles comprised of phosphatidylcholine or phosphatidylcholine/phosphatidylethanolamine mixture. However, ApoL1 confers chloride permeability to vesicles comprised of phosphatidylcholine/phosphatidylserine and phosphatidylcholine/phosphatidic acid vesicles. Thus it appears that ApoL1 requires the presence of negatively charged phospholipids for its chloride permease activity, in agreement with prior reports (8).

Potassium permeability assay

Based on the report of Thomson and Finkelstein (6), we looked for ApoL1-dependent potassium permeability with membrane association at low pH and an efflux assay at neutral pH, using chloride ionophore 1 (CI1) (11) to detect potassium permeability. Representative raw data traces are shown in Fig. 5. In analogy to the tracing shown in Fig. 3, the difference in rates between ApoL1 and control vesicles after addition of CI1 represents the ApoL1-dependent potassium permeability. In contrast to the rather selective chloride permeability shown in Fig. 3, the detectable preionophore efflux here indicates that the ApoL1-conferred permeability is not perfectly potassium-selective. This is consistent with the non-zero val-dependent efflux under the same pH shift conditions as noted above.

Potassium permease activity is linearly dependent on the mass of ApoL1 in the assay (Fig. 6*A*). The eluate from the S200 column was assayed for potassium permeability, and the results are plotted in Fig. 1*D*. The activity peaks with the ApoL1 protein. Potassium-selective permeability requires the presence of calcium ions in both stages of the assay, as shown in Fig. 6*B*;

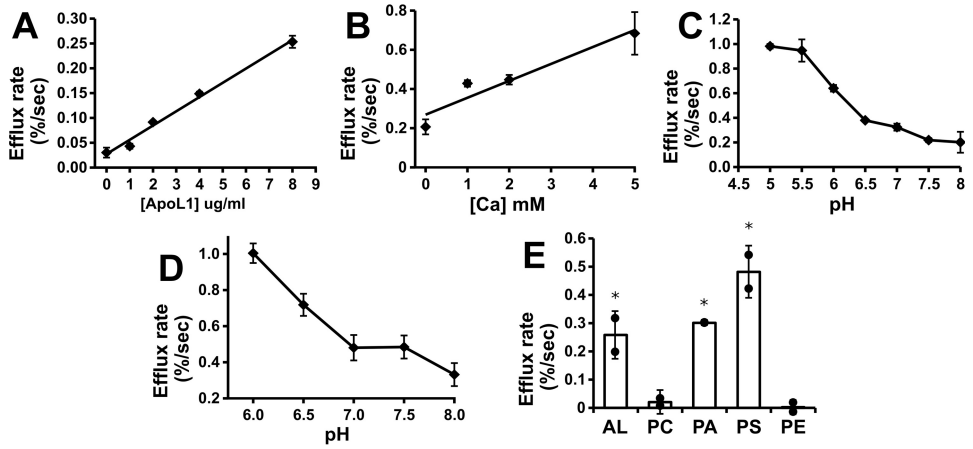

Figure 4. Characterization of the ApoL1-dependent chloride permeability. *A*, ApoL1 concentration dependence. Efflux assays were performed with a range of ApoL1 concentrations in the initial reaction mix at pH 5.0. To eliminate the possibility of buffer or detergent effects, the total volume of S200 buffer solution added to the reaction was held constant. Data points represent the mean, and *error bars* represent S.E.; $n = 2$ for each data point. *B*, calcium dependence. Assays were carried out with 3.8 μg/ml of ApoL1 in the initial reaction mixture at a range of calcium ion concentrations and buffered at pH 6.0 in both stages of the assay. Data points represent mean efflux rates above no-ApoL1 controls, and *error bars* represent S.E.; $n = 2$ for each data point. *C*, pH dependence. Assays were performed with both stages of the assay held at the indicated pH in the presence of 2.5 mM calcium in the presence and absence of ApoL1. Data points represent the mean ApoL1-dependent efflux rates above control vesicles at each pH, and *error bars* represent S.E.; $n = 2$ for each data point. *D*, two-stage pH dependence assay. Vesicles and protein (or control buffer) were mixed at pH 6.0, passed through the spin column, and then assayed for val-dependent efflux at a range of pH values between 6 and 8. Data points and statistics are as in *C*. *E*, lipid dependence. Protein (8 μg/ml final) or control buffer was mixed at pH 5 with vesicles comprised of various combinations of purified lipids and assayed for val-dependent efflux in the absence of calcium. Data points represent individual ApoL1-dependent efflux rates above the control rate for each vesicle mixture. *Columns* represent the mean, *error bars* represent standard deviation; $n = 2$ for each data point. *, $p < 0.05$ compared with the no-protein control rate, determined with t testing. *AL*, asolectin.

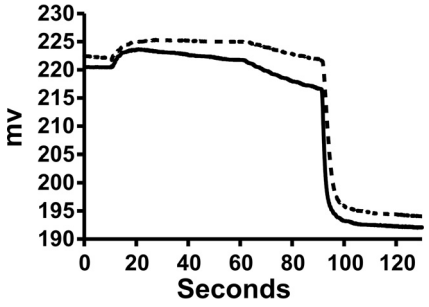

Figure 5. Representative raw data from potassium permease assays. Traces from ApoL1 (*solid line*) and buffer control (*dotted line*) reactions are shown. The initial mixture of protein and vesicles was at pH 6, and the efflux was at pH 7.5. As in Fig. 2, the upward deflection at about 10 s reflects the addition of the Bio-gel P-6DG eluate with dilution of the chloride in the cup. Cl1 is added at 60 s, initiating voltage-driven KCl efflux. Triton X-100 is added at 90 s, releasing all remaining intravesicular chloride. The noticeable chloride release before addition of Cl1 in the ApoL1 sample but not the control indicates the presence of some ApoL1-dependent permeability to both potassium and chloride. The difference in initial rates of release after addition of Cl1 is taken as the ApoL1-dependent potassium permeability.

unlike the chloride permease activity, there is no significant potassium permeability above control in the absence of calcium. Also unlike the chloride permease activity, potassium permeability is sensitive to the intravesicular (trans) pH (Fig. 6*B*), with robust activity when the intravesicular pH is buffered at 8.0 but much less activity when the intravesicular pH is buffered at 6.0. The potassium permease activity of ApoL1 is also dependent on the lipid composition of the vesicles (Fig. 6*C*), requiring the presence of negatively charged lipids, as was found for the chloride permease activity.

ApoL1-conferred potassium permeability is sensitive to extravesicular (*cis*) pH in both stages of the assay, holding the intravesicular (trans) pH at 8.0. Dependence on the cis pH of the association step, followed by efflux at pH 7.5, is shown in Fig. 7 (*solid line*). Activity is greatest in the association stage of the assay at pH 5.5–6.0 and dramatically suppressed above pH 6.5. Dependence on the cis pH of the efflux stage of the assay when association is carried out at pH 6.0 is shown in Fig. 7 (*dashed line*). After association at pH 6.0, potassium permeability is greatest at pH 7.5 and greatly suppressed below pH 7.0.

To summarize the activity experiments, ApoL1 confers ion-selective permeability to phospholipid membranes when allowed to associate with vesicles at low pH. The activity is selective for chloride when the extravesicular pH is held below pH 6.5, but after switch to neutral pH, chloride permeability is suppressed, and potassium permeability is activated.

ApoL1 demonstrates binding to phospholipid vesicles that is sensitive to pH and vesicle lipid composition

The ion permease activity of ApoL1 resulting from direct mixing of protein with preformed lipid vesicles suggests that the protein is able to spontaneously insert into lipid bilayers and span the membrane as an integral membrane protein. To test this hypothesis, we carried out a membrane insertion assay. Purified ApoL1 was mixed with vesicles. After a period of incubation, peripheral membrane proteins were removed by extraction with sodium carbonate (pH 11). The vesicles were then separated from non-inserted or insoluble/aggregated protein by floating the vesicles on top of a sucrose cushion. Vesicles were collected, and one-half of each sample was probed for the presence of ApoL1 by Western blotting.

The results are shown in Fig. 8. Approximately one-third of the ApoL1 in the reaction associates with asolectin vesicles at low pH (Fig. 8*A*, *lanes A*). The fraction that remains after the carbonate wash is taken as that which is inserted into the membrane as an integral membrane protein; in this experiment, it amounts to about 20% of the total protein in the reaction mixture (Fig. 8*A*, *lanes B*). Carrying out the association reaction at pH 8 results in much less carbonate-resistant association (Fig.

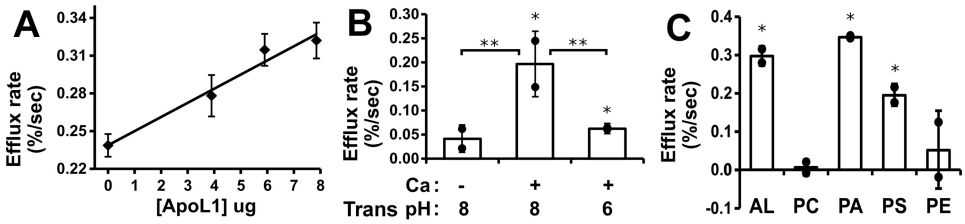

Figure 6. Characterization of ApoL1-dependent potassium permeability. *A*, ApoL1 concentration dependence. Efflux assays were performed with a range of ApoL1 concentration in the initial reaction mix at pH 6, and then efflux was assayed at pH 7.5. To eliminate the possibility of buffer or detergent effects, the total volume of S200 buffer solution added to the reaction was held constant. Data points represent the mean, and *error bars* represent S.E.; $n = 2$ for each data point. *B*, calcium and trans pH dependence of activity. Assays were performed with and without ApoL1, with initial reaction at pH 6 and efflux at pH 7.5, in the absence or presence of 2 mM calcium using vesicles with the internal compartment buffered at 8 (*left* and *center*) or in the presence of 2 mM calcium using vesicles with the internal pH buffered at either 8 or 6 (*center* and *right*). *C*, lipid dependence of potassium permease activity. ApoL1 or control buffer was mixed at pH 6.0 with vesicles comprised of various combinations of purified lipids and assayed for Cl1 dependent efflux at pH 7.5. Lipid mixtures are labeled as in Fig. 4*E*. *B* and *C*, individual data points show the ApoL1-dependent rate above the no-protein control rates for each condition. *Columns* represent the mean, and *error bars* represent standard deviation; $n = 2$ for each data point. *, $p < 0.05$ compared with the no-protein control rate; **, $p < 0.05$ for the pairwise comparisons indicated by *brackets*; significance was determined using ANOVA.

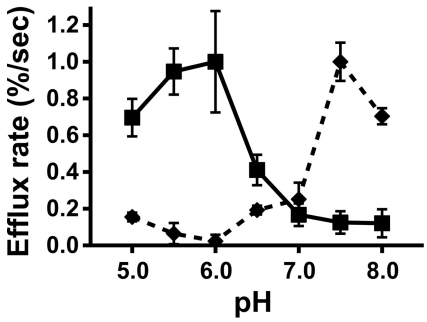

Figure 7. pH Dependence of potassium permease activity. ApoL1 or control buffer was mixed with vesicles at a range of pH values and then assayed for Cl1-dependent efflux at pH 7.5 (*square markers*, *solid line*) or mixed at pH 6.0 and then assayed for Cl1-dependent efflux at a range of pH values (*diamond markers*, *dotted line*). Each point represents the ApoL-1 dependent efflux rate above matched buffer controls; *error bars* represent S.E., $n = 2$ for each data point. Activity is greatest when protein and vesicle association occurs at pH 6.0 and efflux occurs at pH 7.5.

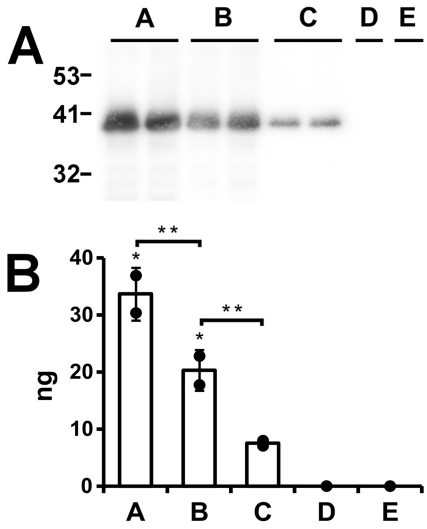

Figure 8. Stable association of ApoL1 with asolectin vesicles. *A*, 0.2 μg of ApoL1 was mixed with preformed vesicles at pH 5 (*lanes A*, *B*, *D*, and *E*) or at pH 8 (*lane C*). Vesicles were then extracted with 100 mM sodium carbonate (pH 11) to remove non-stably bound protein (*lanes B–E*) or not (*lane A*). Vesicles were separated from unbound protein by flotation through sucrose, and half of each sample was then separated by SDS-PAGE, blotted, and probed. Digital images were collected and quantitated using ApoL1 standard separated on the same gel. *Lanes A–C* were performed with independent duplicates. *Lanes D* and *E* are negative controls from which either the protein (*lane D*) or the lipid (*lane E*) was omitted. Migration positions of molecular mass standards in kilodaltons are marked. *B*, quantification of the signals shown in *A*. At pH 8, approximately one-third of the ApoL1 in the reaction bound to the vesicles (*lane A*). A fraction of the membrane-associated protein was extracted with a carbonate wash, leaving behind about 20% of the total protein in the reaction stably associated with the membranes (*lane B*). In contrast, only 7.5% of the total protein stably associates with the vesicles when association is carried out at pH 8.0 (*lane C*). No signal is detected when either protein or lipid is omitted from the reaction. Individual data points are shown. *Columns* represent the mean, and *error bars* represent standard deviation; $n = 2$ for *lanes A–C*. *, $p < 0.05$ (signals significantly different from zero); **, $p < 0.05$ for the pairwise comparisons indicated by *brackets*; significance was determined by ANOVA.

8*A*, *lanes C*). There is no detectable signal in the absence of either ApoL1 (Fig. 8*A*, *lane D*) or vesicles (Fig. 8*A*, *lane E*).

A full pH sensitivity curve of binding is shown in Fig. 9*A*. Membrane insertion is strongly pH-sensitive, with a strong signal at pH 5 dwindling to very little membrane insertion above pH 6.5. There is less binding at all pH values in the absence of calcium (Fig. 9*A*, *dashed line*). Membrane insertion shows the same sensitivity to membrane lipid composition as the activity assays, requiring the presence of negatively charged lipids for robust membrane insertion (Fig. 9*B*).

Intrinsic fluorescence reveals a structural change of ApoL1 when mixed with vesicles at low pH

We used intrinsic fluorescence to probe the secondary/tertiary structure of refolded ApoL1. Tryptophan has the greatest fluorescence intensity of the naturally occurring amino acids, and its fluorescence intensity and the emission wavelength at which its fluorescence intensity is maximal (λ_{max}) are very sensitive to the microscopic environment (12). Hydrophobic environments tend to increase Trp fluorescence intensity and shift λ_{max} to longer wavelength. Thus, conformational transitions that modify the tertiary and/or secondary structure often change the fluorescence of Trp residues within proteins. ApoL1 contains six Trp residues, four in the hypothesized pore-forming region. Trp intrinsic fluorescence was used as spectral reporter to monitor conformational transitions of ApoL1. As a control, we observed that the fluorescence of oligo-tryptophan is not significantly affected by pH between 5.0 and 8.0 (data not shown). We recorded the fluorescence spectra of ApoL1 at a pH range of 5.0–8.0 in the presence and absence of phospholipid vesicles (Fig. 10) and determined difference spectra between the presence and absence of protein. Fig. 10*A* shows the fluorescence emission spectra of identical dilutions of ApoL1 in the presence of phospholipid vesicles at various pH values. Fig. 10*B*

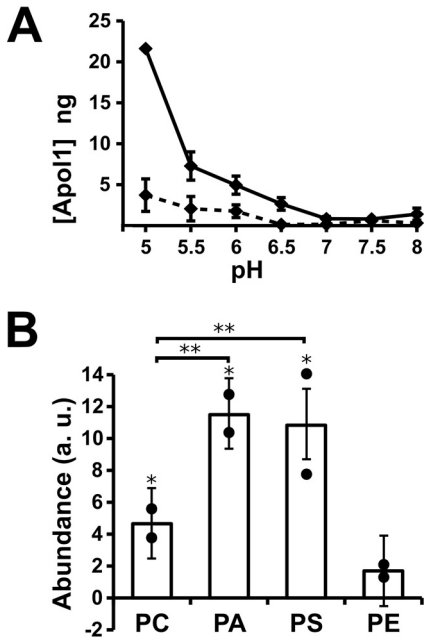

Figure 9. pH and lipid dependence of ApoL1-vesicle association. *A*, the ApoL1 vesicle association assay was performed at a range of pH values in the presence (*solid line*) or absence (*dashed line*) of 5 mM $CaCl_2$. Data points represent the mean, and *error bars* represent S.E., $n = 2$ for each data point. *B*, vesicle association using purified lipid mixtures. Individual data points are shown. *Columns* represent the mean, and *error bars* represent standard deviation; $n = 2$ for each condition. *, $p < 0.05$ compared with zero; **, $p < 0.05$ for the pairwise comparisons indicated by *brackets*; significance was determined by ANOVA.

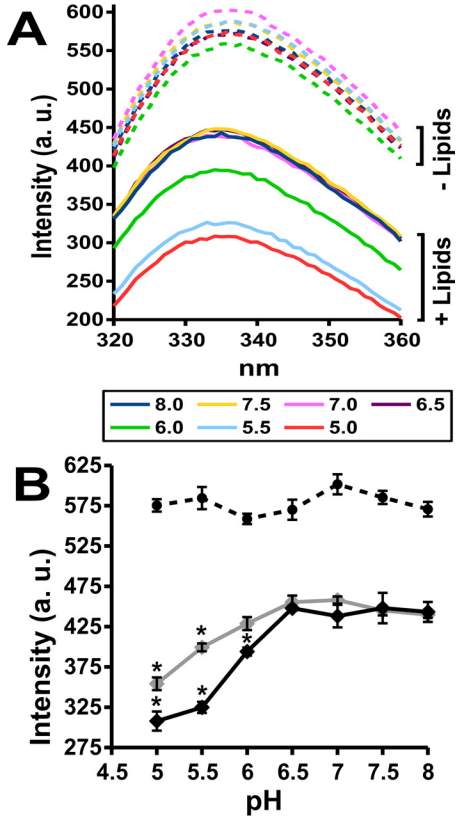

Figure 10. ApoL1 intrinsic fluorescence changes with membrane association. *A*, average fluorescence intensity (*a.u.*, arbitrary units) emission spectra ($\lambda_{ex} = 280$) for ApoL1 in the absence or presence of lipid vesicles at a range of pH values. Each tracing is the average of three identical samples. The pH of each tracing is indicated by color. *B*, fluorescence intensity of ApoL1 at $\lambda_{em} = 335$ through a range of pH values in the presence (*solid line*) or absence (*dashed line*) of vesicles. Fluorescence in the presence of lipids was determined in the presence (*black line*) or absence (*gray line*) of 5 mM $CaCl_2$. Data points represent the mean value, and *error bars* represent S.E.; $n = 3$ for each data point. *, $p < 0.05$ compared with intensity at pH 6.5 within each data set determined by ANOVA.

plots the fluorescence intensity at 335 nm in the presence or absence of lipid vesicles. In the absence of vesicles, pH has little effect on ApoL1 intrinsic fluorescence (Fig. 10*B*, *dashed line*). This may reflect no change in the environment of any of the Trp residues or multiple changes that cancel each other out in the aggregate. In contrast, in the presence of phospholipid vesicles, lowering the pH below 6.5 results in a progressive decrease in total fluorescence, suggesting that at least some of the endogenous Trp residues transition from a less to a more polar environment (Fig. 10*B*, *solid black line*). Of note, this is the same critical pH range during association that supports development of both chloride and potassium ion permeability and where association with vesicles in increased. The decrease in fluorescence is smaller in the absence of calcium (Fig. 10*B*, *solid gray line*). We did not detect a significant pH-dependent shift of λ_{max} in either the presence or absence of lipid vesicles.

Discussion

We have investigated the biochemical properties of purified recombinant ApoL1 and generated novel data that expand our knowledge of this important protein. We used vesicle-based voltage-driven permeability assays to characterize the transport properties of ApoL1 added directly to preformed phospholipid vesicles. We found that ApoL1 spontaneously enters into vesicles at low pH and confers chloride-selective permeability when the pH remains low. If the extravesicular pH is raised to neutral, then the chloride permeability is suppressed, and a cation permeability is activated. Both chloride and potassium permease activities co-elute with ApoL1 on gel exclusion chromatography, and both are linearly dependent on the amount of ApoL1 added to the assay, supporting the notion that both of these activities are due to ApoL1 itself. Potassium permeability requires the presence of calcium throughout the assay; chloride permeability does not require the presence of calcium but is enhanced when calcium is present. Both chloride and potassium permease activities show marked sensitivity to membrane composition, requiring the presence of negatively charged phospholipids. Using a membrane association assay, we find that ApoL1 stably associates with phospholipid vesicles in a pH- and lipid-dependent pattern that correlates with the activity assays. Intrinsic fluorescence studies indicate that ApoL1 goes through a significant structural transition in the presence of vesicles under conditions that induce membrane insertion. Taken together, the data support the conclusion that ApoL1 can enter membranes at low pH and form a pH-switchable ion-selective permease.

These data bridge the gap between individual reports of anion-selective permeability conferred by ApoL1 at low pH and cation-selective channel activity after insertion at low pH followed by titration to neutral. In particular, our anion permeability and membrane association data agree well with the report from Harrington *et al.* (8), whereas our potassium permeability

data are in agreement with the bilayer data of Thomson and Finkelstein (6). Our data strongly support the notion that both the anion and cation permease activities are properties of ApoL1 itself.

pH-switchable ion selectivity could account for the reported effects of ApoL1 in both the endosomal pathway and on the plasma membrane. Following uptake of ApoL1 by endocytosis, acidification of endosomes would trigger membrane insertion and induction of anion-selective permeability. The consequences of increased anion permeability along the endocytic pathway will depend on the anion selectivity of the permease: chloride-selective permeability may enhance acidification of the endocytic compartment when proton pump activity is limited by counterion movement. Alternatively, non-selective anion permeability (allowing bicarbonate transfer) would be expected to collapse the pH gradient across the endosomal membrane with increased steady-state endosomal pH. Either way, alterations in endosomal pH could contribute to the effects on endosomal–lysosomal function that have been reported in both trypanosomes and mammalian cells (5, 13–20).

ApoL1, which has inserted into the endosomal membrane as a consequence of endosomal acidification, could subsequently be targeted to the plasma membrane or other compartments in which the extracytoplasmic topological surface is at neutral pH. This pH transition would suppress anion permeability and activate cation channel activity, leading to the plasma membrane non-selective cation permeability reported in both trypanosomes and cultured cells (6, 9).

Which activity dominates could be a consequence of the source of ApoL1. Exogenous ApoL1 delivered to the cell via endocytosis would have access to the entire endocytic–lysosomal and recycling pathways, where the insertion and anion permeability induced by the acidic environment could result in the pleiotropic effects on intracellular compartments reported for ApoL1. In contrast, endogenous expression of ApoL1 with its N-terminal signal sequence would result in delivery of the molecule to the exocytic pathway. Vesicles along the exocytic pathway also acidify, which could induce membrane insertion prior to delivery to the plasma membrane and/or other membrane-bound compartments, depending on targeting signals that may be present. Thus, in human cells, one might expect endogenously expressed ApoL1 to have predominantly cell surface/cell depolarization effects, whereas uptake of exogenous ApoL1 via endocytosis may predominately have effects on the endocytic, recycling, and lysosomal compartments. Whether ApoL1 acts via autocrine or paracrine routes may be critically important to its cellular consequences.

The structure of the N-terminal domain of ApoL1 has been proposed to bear secondary structural similarity to the pore-forming domain of the family of pore-forming porins (5, 20), which have been studied extensively (21). Porins are thought to form channels in a two-step process. Initial membrane insertion occurs with an α-helical loop formed from helices 8 and 9 inserting into and traversing the membrane, with the turn of the hairpin exposed on the trans face of the membrane (22, 23) and the remaining parts to the molecule remaining on the cis side, where amphipathic helices also contribute significantly to membrane association (24). Although the details are uncertain, channel opening is thought to be associated with more substantial transfer of portions of the protein into and across the bilayer, with as much as α helices 2 through 5 exposed on the trans side of the membrane (21, 25).

Using colicin structure as a starting point, our data have some structural implications for ApoL1. First, we observed that the protein can insert into the membrane at low pH in the cis compartment, but development of cation permeability after titration back to neutral is dependent on the pH of the trans compartment. This suggests an "ion trapping" model of stable membrane insertion (26) in which a titratable carboxylic acid residue of the protein can be protonated at low pH, removing the charge from that amino acid residue and facilitating translocation of part of the protein through the lipid bilayer and exposure on the trans side of the membrane. If the trans compartment is held at neutral pH, the carboxylic acid residue can lose its proton and assume a negative charge, preventing the protein from leaving the membrane and essentially locking it in place. In analogy to channel-forming porins, helices 8 and 9 are predicted to from a transmembrane loop upon membrane insertion. Glutamic acid at 209 would be predicted to be exposed to the trans compartment and could be playing the ion-trapping role.

A second structural implication derives from the intrinsic fluorescence. Titration of ApoL1 to a pH below 6 in the presence of phospholipid vesicles results in decreased fluorescence, indicating a transition of one or more of the Trp moieties in the protein to a more polar environment. Curiously, this loss of fluorescence intensity only occurs in the presence of lipid. Thus, this is not simply a pH-driven structural transition that forces a Trp to interact with the aqueous environment (which would occur independent of the presence of lipid) but, rather, that membrane insertion drives one or more Trps into a polar environment in the vesicles, suggesting an interaction between Trp residues and the polar headgroups of the phospholipid membrane. Again using the proposed porin-like structure as a guide, we predict that the two tryptophans at positions 234 and 235, which are at the end of helix 10, are likely to be in the vicinity of the polar surface of the membrane and may be responsible for the decreased intrinsic fluorescence signal on membrane insertion. Trp residues at position 94 in the middle of helix 2, at position 129 between helices 3 and 4, and at position 139 within helix 4 could also potentially be in the proximity of the phospholipid polar headgroups in the membrane-inserted form.

Activation of cation permeability requires titration of the cis compartment to neutral after the protein has inserted from the cis compartment at low pH. This suggests that an ionizable group that is titrated between pH 6 and 7.5 is exposed to the cis compartment and whose titration is necessary for cation channel activity. The histidines at positions 130, between proposed helices 3 and 4, and at position 169 in helix 6 would be candidates for the pH sensor.

The contrast between the pH sensitivity of conditions for insertion leading to anion or cation permeability is also of interest. Chloride permeability increases as the pH falls to 5.0 (the lowest pH investigated), and this matches well with overall

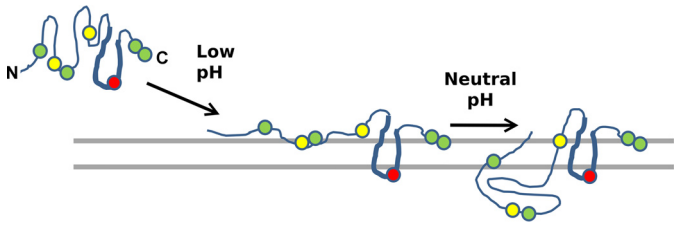

Figure 11. Working model for membrane insertion of the ApoL1 pore-forming domain. Only the putative pore-forming domain (amino acids 90–235) is shown. At neutral pH, ApoL1 is folded in a soluble conformation (*left*). With titration of the cis compartment to acidic pH, the hairpin loop formed by helices 8 and 9 (indicated by the *thickened line segment*) inserts into and spans the membrane, exposing glutamic acid 209 (*red circle*) to the trans aqueous environment, where it could be titrated, and forcing tryptophans at positions 234 and 235 and/or 94 and/or 139 (*green circles*) to interact with the lipid polar headgroups on the cis side of the membrane (*center*). This form confers chloride permeability, perhaps via membrane disruption at the protein–lipid interface. Titration of the cis compartment back to neutral pH, possibly with histidines at positions 130 and 169 serving as the pH sensor, drives the further conformational change and translocation leading to potassium permeability (*right*) (structures per 5, 20, 21 with modifications).

membrane insertion, which also increases as the pH is decreased to 5.0. However, the optimal pH of membrane association leading to potassium permeability is 6.0, and the activity falls when the pH during the association step is decreased further to 5, despite the fact that more protein binds as the pH falls below 6.0. This observation suggests that not all of the protein that inserts into the membrane and supports anion permeability at low pH is competent to go through the transition leading to cation selective activity at neutral pH. Insertion at lower pH thus drives the protein into a conformation that can still support anion permeability but from which it cannot convert to the cation-selective channel form when the pH is brought back to neutral. Perhaps titration of additional carboxylic acid groups, of which there are many in the pore-forming domain, render the conformation supporting anion permeability to be irreversible.

Because our transport data are entirely from vesicle-based flux experiments, they are silent on whether the observed ion selective permeabilities are due to well-behaved gated pores or perhaps a more general disruption of the lipid bilayers. It is relevant to note the observations of Thomson and Finkelstein (6) of increased permeability of the planar lipid bilayers when ApoL1 was introduced at low pH before titration back to neutral. Discrete channel transitions were not observed, and ion selectivity of this was not reported. This may correspond to the anion-selective permeability we observe under similar conditions. Like Thomson and Finkelstein (6), we also note induction of potassium-selective permeability when membrane-inserted protein formed at low pH is brought to neutral and, by analogy, expect that this activity is due to the gated channel activity they observed in the bilayer.

We propose that ApoL1 enters the membrane at low pH, perhaps, in analogy to colicins, by insertion of the α-helical loop formed from helices 8 and 9 (diagrammed in Fig. 11). This structure disrupts the membrane in a specific way that induces anion-selective permeability, but not necessarily through a well-behaved gated pore. Such permeability could be the result of a pore forming at the protein–lipid interface (27, 28). Titration of the cis chamber back to neutral induces a further structural transition that results in activation of a cation-selective gated channel. Again in analogy to colicins, this pH-triggered transition could be the transfer of helices 2–5 to the trans face of the membrane and possible formation of a protein-lined water-filled pore. Although the porin model seems attractive, there is to date very little published evidence supporting the idea that it applies in any detail to ApoL1, and certainly other domains of the ApoL1 molecule could be contributing to membrane binding and permease activity.

Accumulating data indicate that the cation-selective channel activity of ApoL1 has important cellular consequences. Whether the anion-selective permeability occurring with membrane insertion at low pH is biologically relevant remains to be seen but could well account for the many pleiotropic effects on intracellular membranes that have been reported in both trypanosomes and cultured mammalian cells. A major unanswered question is whether the disease-associated variants alter the membrane association and ion permease activities of ApoL1 and whether any such changes contribute to the accelerated renal disease observed in people carrying those genetic variants.

Experimental procedures

Expression construct

ApoL1-encoding plasmid was derived from clone 40148156 purchased from Open Biosystems (now GE Dharmacon) using combinations of subcloning, gene synthesis (using the services of Integrated DNA Technologies Inc.), and PCR with mutagenic primers. The identities of the final products generated by synthesis or PCR were confirmed by direct sequence determination.

pET-ApoWT was independently derived but functionally identical to the expression construct reported by Thomson and Finkelstein (6), consisting of the coding region for mature ApoL1 (starting with the codon for amino acid 28) preceded immediately by a BamHI site and extending through the entire ApoL1 coding region and the endogenous stop codon to an XbaI-XhoI multicloning restriction site cluster created 27 bases downstream of the stop codon, inserted into the BamHI-XhoI sites of pET28a. This construct thus encodes mature ApoL1 from amino acids 28 through 398 with an N-terminal His_6 affinity tag and T7 epitope tag, under the control of a T7 promoter for high-level expression in *Escherichia coli*. The predicted molecular mass of the encoded fusion protein is 44,488.

Expression and purification from pET-ApoWT

Overnight cultures of BL21(DE3) bacteria carrying pET-ApoWT in non-autoinducing medium were used to inoculate 100 ml of autoinduction medium and grown overnight at 37 °C with shaking (29). Preparation of washed insoluble inclusion bodies was as described previously (6). The pellet was suspended in 140 ml of 1% Zwittergent 3-14 (Millipore) in water. While stirring, we added 140 μl of 10 N NaOH was added , and we allowed it to stir for 2.5 min, during which the solution clarified dramatically. Sodium chloride was added to 150 mM, and Tris base was added to 10 mM. Tris-HCl was added dropwise with stirring to 10 mM, and the solution was then titrated to pH 8.3 with concentrated HCl. After stirring for 5 min, the

sample was centrifuged at 100,000 × *g* for 45 min. The supernatant was loaded onto a nickel-agarose column equilibrated with 20 mM Tris (pH 8), 150 mM NaCl, and 1% Zwittergent, washed in the same solution supplemented with 20 mM imidazole, followed by 20 mM Tris (pH 8), 150 mM NaCl, 20 mM imidazole, and 0.3% Zwittergent, and then eluted with 20 mM Tris (pH 8.0), 150 mM NaCl, 300 mM imidazole, and 0.3% Zwittergent. Peak fractions from the high-imidazole elution were pooled, and 4 ml was loaded onto an ~100-ml Sephacryl S200 HR column equilibrated and eluted with 10 mM HEPES (pH 8), 150 mM NaCl, and 0.02% DDM.

Trypanosome viability assay

T. brucei brucei, Lister 427, were maintained in HMI-9 growth medium. Parasites were plated in 50 μl of growth media into a white 96-well plate. Serial dilutions of ApoL1 were added at 2× their final concentration in 50 μl of growth medium. Parasites were incubated for 24 h in the presence of ApoL1, and trypanosome viability was assessed using a Cell-Titer-Glo assay (Promega). Data were fit to a Boltzmann equation to determine the LC_{50} using MicroCal Origin.

Vesicle efflux assays

Efflux assays were performed essentially as described previously (10). Unless otherwise noted, vesicles were prepared from asolectin (soybean phosphatidyl choline type II, Sigma) that had been acetone-extracted as described previously (30) or from purified phospholipids (Avanti Polar Lipids). Purified lipid mixtures were as follows: PC (90% phosphatidyl choline, 10% cholesterol), PA (80% phosphatidyl choline, 10% phosphatidic acid, and 10% cholesterol), PS (80% phosphatidyl choline, 10% phosphatidyl serine, and 10% cholesterol), and PE (80% phosphatidyl choline, 10% phosphatidyl ethanolamine, and 10% cholesterol). Phospholipids in chloroform were dried and suspended at 20 mg/ml in 200 mM KCl with 5 mM buffer (HEPES (pH 8.0) or MES (pH 5.0)) by repeated freeze–thaw cycles and then passed 15 times through a 200-nm pore membrane filter to generate unilamellar vesicles. A 380-μl reaction mixture was assembled from 156 μl of 200 mM KCl, 148 μl of 330 mM sucrose (isotonic to 200 mM KCl), 32 μl of 0.5 M buffer stock, 8 μl of 100 mM $Ca(gluconate)_2$, and 35 μl of 20 mg of lipid vesicle suspension. Twenty microliters of ApoL1 preparation or identical control buffer was added with stirring. Unless otherwise noted, the final composition of the reaction mix was 95.5 mM KCl, 7.5 mM NaCl, 111 mM sucrose, 40 mM buffer (MES or HEPES), 2 mM $Ca(gluconate)_2$, 1.75 mg/ml asolectin vesicles, and 0.001% DDM. The final DDM concentration was well below the critical micelle concentration, and did not affect the ionic leakiness of the vesicles. The mixture was incubated at room temperature for 5 min and then passed through a 3.5-ml Bio-gel P-6DG (Bio-Rad) spin column equilibrated with 330 mM sucrose. The ~0.5 ml of eluate of the spin column was immediately added to a cup containing 2 ml of 10 mM buffer, 10^{-5} M KCl, and 2.0 mM $Ca(gluconate)_2$ in 330 mM sucrose, which was being continuously monitored with an Accumet chloride-selective electrode attached to a Jenco pH meter that was interfaced through a Digidata 1200 A-D converter and a WPI low-pass filter (LPF-30) filtered at 200 Hz to a computer running Axoscope. After the recording stabilized (45–60 s), voltage-driven efflux was initiated by addition of 2.5 μl of ionophore (1 mM val or 0.2 mM CI1 (both from Sigma)) in ethanol and allowed to proceed for 30 s. Twenty-five microliters of 10% Triton X-100 was added to release the remaining intravascular chloride. The data in millivolts were converted to chloride concentration using a standard curve generated for the electrode. Fractional release of chloride over 5 s immediately following addition of the ionophore was taken as the vesicle ion permeability.

Membrane association

4 μl of asolectin vesicles (prepared as for the efflux assay) and 0.2 μg of ApoL1 in 4 μl (or 4 μl of control buffer) were added to 42 μl reaction mixture comprised of 100 mM KCl, 165 mM sucrose, 40 mM buffer (HEPES or MES), and 2.4 mM Ca(gluconate)$_2$ and incubated for 1 min. 150 μl of $NaCO_3$ was added to a final concentration of 100 mM (accounting for titration by buffer). After incubation at room temperature for 15 min, 0.8 ml of 50% sucrose was added. The sample was layered beneath a two-stage step gradient with a 1-ml lower phase of 30% sucrose and 2.7-ml upper phase of water (both with 8 mM HEPES (pH 7.5)). The gradient was spun at 200,000 × *g* for 90 min at 4 °C in a Beckman TLA-110 rotor. The vesicles were collected from the interface between the upper and middle phases. Half of the sample was diluted 1:1 with 8 mM HEPES (pH 8) in water and centrifuged at 100,000 × *g* for 45 min. The pellet was dissolved in loading buffer, separated by sodium dodecyl sulfate polyacrylamide gel electrophoresis, and blotted to PDF membranes by standard techniques. Blots were developed with anti-T7 epitope primary antibody (Millipore) and horseradish peroxidase–conjugated goat anti-mouse antibody (Thermo Fisher) using Supersignal West Dura (Thermo Fisher) chemiluminescence reagent and detected with a Protein Simple Fluorochrome M digital imaging system. Serial dilutions of stock ApoL1 solutions were separated on the same gel to confirm the linearity of the signal and allow quantification using AlphaView SA software.

Intrinsic fluorescence

20 μl of ApoL1 stock or control S200 buffer was diluted to 0.5 ml in 330 mM sucrose, 10 mM MES/HEPES buffer, 5 mM $CaCl_2$, and with or without asolectin vesicles at 0.4 mg/ml final concentration. The final protein concentration was 6 μg/ml. Fluorescence emission spectra were collected with excitation at 280 nm and emission from 320 to 350 nm using a Cary Eclipse fluorescence spectrophotometer. Three independently prepared samples for each data point were scanned in triplicate, and signals were averaged. Difference spectra were determined by subtracting signals in the absence of ApoL1 from the corresponding spectra with ApoL1.

Author contributions—J. C. E. conceived and organized the project, performed the molecular biology and efflux experiments, and wrote the paper. J. B. performed the purification, membrane association, and intrinsic fluorescence experiments and generated the figures. N. P. provided advice and interpretation of the intrinsic fluorescence studies. J. O. performed the trypanosome viability assay.

Acknowledgment—We thank Russell Thomson (Albert Einstein College of Medicine) for helpful discussions.

References

1. Genovese, G., Friedman, D. J., Ross, M. D., Lecordier, L., Uzureau, P., Freedman, B. I., Bowden, D. W., Langefeld, C. D., Oleksyk, T. K., Uscinski Knob, A. L., Bernhardy, A. J., Hicks, P. J., Nelson, G. W., Vanhollebeke, B., Winkler, C. A., *et al.* (2010) Association of trypanolytic ApoL1 variants with kidney disease in African Americans. *Science* **329,** 841–845
2. Parsa, A., Kao, W. H., Xie, D., Astor, B. C., Li, M., Hsu, C. Y., Feldman, H. I., Parekh, R. S., Kusek, J. W., Greene, T. H., Fink, J. C., Anderson, A. H., Choi, M. J., Wright, J. T., Jr., Lash, J. P., *et al.* (2013) APOL1 risk variants, race, and progression of chronic kidney disease. *N. Engl. J. Med.* **369,** 2183–2196
3. Pays, E., and Vanhollebeke, B. (2008) Mutual self-defence: the trypanolytic factor story. *Microbes Infect.* **10,** 985–989
4. Vanhamme, L., Paturiaux-Hanocq, F., Poelvoorde, P., Nolan, D. P., Lins, L., Van Den Abbeele, J., Pays, A., Tebabi, P., Van Xong, H., Jacquet, A., Moguilevsky, N., Dieu, M., Kane, J. P., De Baetselier, P., Brasseur, R., and Pays, E. (2003) Apolipoprotein L-I is the trypanosome lytic factor of human serum. *Nature* **422,** 83–87
5. Pérez-Morga, D., Vanhollebeke, B., Paturiaux-Hanocq, F., Nolan, D. P., Lins, L., Homblé, F., Vanhamme, L., Tebabi, P., Pays, A., Poelvoorde, P., Jacquet, A., Brasseur, R., and Pays, E. (2005) Apolipoprotein L-I promotes trypanosome lysis by forming pores in lysosomal membranes. *Science* **309,** 469–472
6. Thomson, R., and Finkelstein, A. (2015) Human trypanolytic factor APOL1 forms pH-gated cation-selective channels in planar lipid bilayers: relevance to trypanosome lysis. *Proc. Natl. Acad. Sci. U.S.A.* **112,** 2894–2899
7. Vanwalleghem, G., Fontaine, F., Lecordier, L., Tebabi, P., Klewe, K., Nolan, D. P., Yamaryo-Botté, Y., Botté, C., Kremer, A., Burkard, G. S., Rassow, J., Roditi, I., Pérez-Morga, D., and Pays, E. (2015) Coupling of lysosomal and mitochondrial membrane permeabilization in trypanolysis by APOL1. *Nat. Commun.* **6,** 8078
8. Harrington, J. M., Howell, S., and Hajduk, S. L. (2009) Membrane permeabilization by trypanosome lytic factor, a cytolytic human high density lipoprotein. *J. Biol. Chem.* **284,** 13505–13512
9. Olabisi, O. A., Zhang, J. Y., VerPlank, L., Zahler, N., DiBartolo, S., 3rd, Heneghan, J. F., Schlöndorff, J. S., Suh, J. H., Yan, P., Alper, S. L., Friedman, D. J., and Pollak, M. R. (2016) APOL1 kidney disease risk variants cause cytotoxicity by depleting cellular potassium and inducing stress-activated protein kinases. *Proc. Natl. Acad. Sci. U.S.A.* **113,** 830–837
10. Tulk, B. M., Kapadia, S., and Edwards, J. C. (2002) CLIC1 inserts from the aqueous phase into phospholipid membranes, where it functions as an anion channel. *Am. J. Physiol. Cell Physiol.* **282,** C1103–C1112
11. El-Etri, M., and Cuppoletti, J. (1996) Metalloporphyrin chloride ionophores: induction of increased anion permeability in lung epithelial cells. *Am. J. Physiol.* **270,** L386–L392
12. Ghisaidoobe, A. B., and Chung, S. J. (2014) Intrinsic tryptophan fluorescence in the detection and analysis of proteins: a focus on Forster resonance energy transfer techniques. *Int. J. Mol. Sci.* **15,** 22518–22538
13. Wan, G., Zhaorigetu, S., Liu, Z., Kaini, R., Jiang, Z., and Hu, C. A. (2008) Apolipoprotein L1, a novel Bcl-2 homology domain 3-only lipid-binding protein, induces autophagic cell death. *J. Biol. Chem.* **283,** 21540–21549
14. Zhaorigetu, S., Wan, G., Kaini, R., Jiang, Z., and Hu, C. A. (2008) ApoL1, a BH3-only lipid-binding protein, induces autophagic cell death. *Autophagy* **4,** 1079–1082
15. Kruzel-Davila, E., Shemer, R., Ofir, A., Bavli-Kertselli, I., Darlyuk-Saadon, I., Oren-Giladi, P., Wasser, W. G., Magen, D., Zaknoun, E., Schuldiner, M., Salzberg, A., Kornitzer, D., Marelja, Z., Simons, M., and Skorecki, K. (2017) APOL1-mediated cell injury involves disruption of conserved trafficking processes. *J. Am. Soc. Nephrol.* **28,** 1117–1130
16. Lan, X., Jhaveri, A., Cheng, K., Wen, H., Saleem, M. A., Mathieson, P. W., Mikulak, J., Aviram, S., Malhotra, A., Skorecki, K., and Singhal, P. C. (2014) APOL1 risk variants enhance podocyte necrosis through compromising lysosomal membrane permeability. *Am. J. Physiol. Renal Physiol.* **307,** F326–F336
17. Beckerman, P., Bi-Karchin, J., Park, A. S., Qiu, C., Dummer, P. D., Soomro, I., Boustany-Kari, C. M., Pullen, S. S., Miner, J. H., Hu, C. A., Rohacs, T., Inoue, K., Ishibe, S., Saleem, M. A., Palmer, M. B., *et al.* (2017) Transgenic expression of human APOL1 risk variants in podocytes induces kidney disease in mice. *Nat. Med.* **23,** 429–438
18. Fu, Y., Zhu, J. Y., Richman, A., Zhang, Y., Xie, X., Das, J. R., Li, J., Ray, P. E., and Han, Z. (2017) APOL1-G1 in nephrocytes induces hypertrophy and accelerates cell death. *J. Am. Soc. Nephrol.* **28,** 1106–1116
19. Bruggeman, L. A., O'Toole, J. F., and Sedor, J. R. (2017) Identifying the intracellular function of APOL1. *J. Am. Soc. Nephrol.* **28,** 1008–1011
20. Pays, E., Vanhollebeke, B., Uzureau, P., Lecordier, L., and Pérez-Morga, D. (2014) The molecular arms race between African trypanosomes and humans. *Nat. Rev. Microbiol.* **12,** 575–584
21. Cascales, E., Buchanan, S. K., Duché, D., Kleanthous, C., Lloubès, R., Postle, K., Riley, M., Slatin, S., and Cavard, D. (2007) Colicin biology. *Microbiol. Mol. Biol. Rev.* **71,** 158–229
22. Kienker, P. K., Qiu, X., Slatin, S. L., Finkelstein, A., and Jakes, K. S. (1997) Transmembrane insertion of the colicin Ia hydrophobic hairpin. *J. Membr. Biol.* **157,** 27–37
23. Kienker, P. K., Jakes, K. S., and Finkelstein, A. (2008) Identification of channel-lining amino acid residues in the hydrophobic segment of colicin Ia. *J. Gen. Physiol.* **132,** 693–707
24. Bermejo, I. L., Arnulphi, C., Ibáñez de Opakua, A., Alonso-Mariño, M., Goñi, F. M., and Viguera, A. R. (2013) Membrane partitioning of the pore-forming domain of colicin A: role of the hydrophobic helical hairpin. *Biophys. J.* **105,** 1432–1443
25. Qiu, X. Q., Jakes, K. S., Kienker, P. K., Finkelstein, A., and Slatin, S. L. (1996) Major transmembrane movement associated with colicin Ia channel gating. *J. Gen. Physiol.* **107,** 313–328
26. Kaul, P., Silverman, J., Shen, W. H., Blanke, S. R., Huynh, P. D., Finkelstein, A., and Collier, R. J. (1996) Roles of Glu 349 and Asp 352 in membrane insertion and translocation by diphtheria toxin. *Protein Sci.* **5,** 687–692
27. Gilbert, R. J., Dalla Serra, M., Froelich, C. J., Wallace, M. I., and Anderluh, G. (2014) Membrane pore formation at protein-lipid interfaces. *Trends Biochem. Sci.* **39,** 510–516
28. Whitlock, J. M., and Hartzell, H. C. (2017) Anoctamins/TMEM16 proteins: chloride channels flirting with lipids and extracellular vesicles. *Annu. Rev. Physiol.* **79,** 119–143
29. Studier, F. W. (2014) Stable expression clones and auto-induction for protein production in *E. coli*. *Methods Mol. Biol.* **1091,** 17–32
30. Kagawa, Y., and Racker, E. (1971) Partial resolution of the enzymes catalyzing oxidative phosphorylation: XXV: reconstitution of vesicles catalyzing $^{32}P_i$-adenosine triphosphate exchange. *J. Biol. Chem.* **246,** 5477–5487